Exploring the Photodynamics of a New 2D-MOF Composite: Nile Red@Al−ITQ-HB

Elena Caballero-Mancebo,[†] Boiko Cohen,[†] José María Moreno,[‡] Avelino Corma,[‡] Urbano Díaz,*[,‡] and Abderrazzak Douhal*[,†]

[†]Departamento de Química Física, Facultad de Ciencias Ambientales y Bioquímica, and INAMOL, Universidad de Castilla-La Mancha, Avenida Carlos III, S/N, 45071 Toledo, Spain

[‡]Instituto de Tecnología Química, Universitat Politecnica de Valéncia-Consejo Superior de Investigaciones Científicas (UPV-CSIC), Av. de los Naranjos s/n, 46022 Valencia, Spain

Ⓢ Supporting Information

ABSTRACT: In this work, we unravel the photodynamics of Nile Red (NR) interacting with Al−ITQ-HB nanostructure, a new layer-type metal−organic framework (MOF) with potential catalytic and photonic applications. Steady-state spectroscopy reveals the presence of NR monomers and aggregates when interacting with the MOF structure. Time-resolved experiments provide emission lifetimes of the interacting monomers, H- and J-type aggregates. We observed contributions from two monomer populations having different environments. One monomer species emits from the local-excited state and another from a photo-produced charge-separated state resulting from an ultrafast intramolecular charge transfer (ICT). Femtosecond fluorescence experiments reveal that the ICT process occurs in ∼1 ps. Fluorescence microscopy on single crystals and agglomerates of the composites shows a homogenous distribution of the dye lifetimes within the material. This study shows that the photobehavior of NR in Al−ITQ-HB MOF is dictated by its location within the material. The reported findings using a well-known polarity probe and a new two-dimensional MOF provide information on the microenvironment of this material, which may help for designing smart MOFs with potential applications in photonics and nanocatalysis.
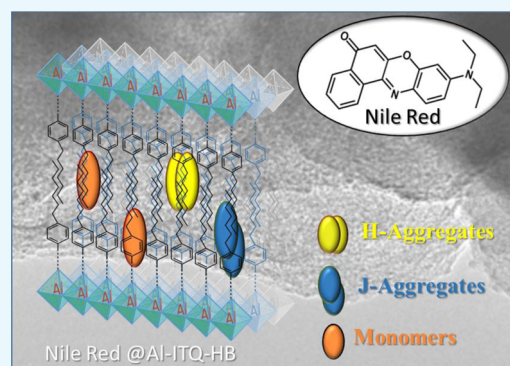
1. INTRODUCTION

One of the interests of the scientific community is currently focused on the development and understanding of new porous materials because of new challenges faced by the modern society.[1−4] Metal−organic frameworks (MOFs) are becoming one of the most promising porous materials because of their wide range of applications[5] in gas storage and separation,[6−10] catalysis,[11,12] drug delivery,[13] magnetic materials,[14] and optoelectronic devices.[15] MOFs are formed by coordinative bonding of multidentate ligands to metal atoms or metal clusters. The resulting network has a large specific area that is distributed among the surface, channels, and pores. The structures of these materials are normally quite rigid, and weak interactions, such as H-bonding or π−π stacking, may provide flexibility to the system.[16] These properties make three-dimensional (3D) MOFs very suitable systems for encapsulating several molecules and having potential applications.[5−15] A special case of the MOF structure is the one based on sheet units, which provides two-dimensional (2D) materials. These structures have larger active surface areas and enable better diffusion of guest molecules.[17−21] Recently, a novel mesostructured metal−organic-type material, based on these ordered metal-cluster sheets (Al−ITQ-HB), has been synthesized.[22] The linker in this structure is 4-heptylbenzoic acid (HB), which interacts with the aluminum metal cluster through the carboxylic group forming stable coordination bonds. The hydrocarbon tail acts as a spacer between the metal nodes, inhibiting the 3D growth and promoting the formation of layers.[23,24] The stability of this MOF in aqueous media and the diffusion of molecules within its structure turns it into a promising material for several applications, such as catalysis.[22]

Nile Red (NR) is a good candidate for studying the properties of the MOF system because of its strong fluorescence and high sensitivity to the properties (i.e. polarity and H-bonding) of the environment.[24−28] It undergoes an intramolecular charge transfer (ICT) reaction in its first singlet excited state (S_1) in tens of femtoseconds[29−31] because of the presence of both amino and keto groups, which have electrodonating and withdrawing characters, respectively. NR has been largely used as a probe to study different environments.[32−36] For example, steady-state studies have shown the presence of different populations (as aggregates and monomers) of NR upon interaction with silica-based materials (SBMs)[37] such as zeolites[28,31] and MCM-41.[29,30]
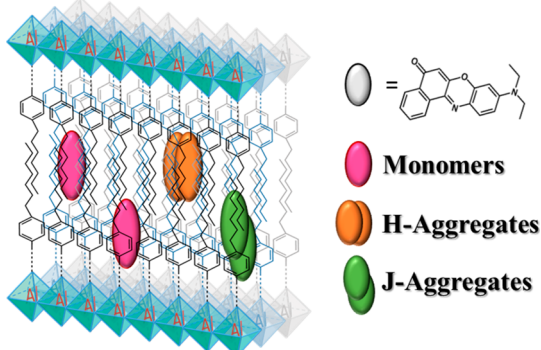
Herein, we report the results of studies on how the photobehavior of NR is affected when it interacts with the Al−ITQ-HB MOF (Scheme 1). Steady-state UV−visible

Scheme 1. Illustration (Not in Scale) of NR Monomers, J- and H-aggregate Distribution within the Al−ITQ-HB Framework

experiments demonstrate the presence of several species. The emission of these populations is affected by the initial dye concentrations in the composites. The shift of the emission to longer wavelengths upon increasing the dye content suggests the formation of aggregates. Time-resolved experiments show the contribution of two differently located monomers and aggregates (J- and H-type), showing that the photobehavior of NR is affected by its location within the MOF. The femtosecond time-resolved emission experiments showed ultrafast formation of a charge-separated (CS) state (∼1 ps), followed by a vibrational cooling (VC) in ∼8 ps. The scanning confocal fluorescence microscopy of single crystals and agglomerates of the composite indicates that the dye is homogenously distributed within the MOF. These results using a well-known polarity probe molecule help in understanding the properties of this novel metal−organic structure Al−ITQ-HB, which may lead to the development of new material designs.

2. RESULTS AND DISCUSSION

2.1. Steady-State Observation of NR@Al−ITQ-HB. We studied the steady-state behavior of NR@Al−ITQ-HB composites in the solid state. The MOF exhibits a band at ∼250 nm and a weak tail up to 600 nm (Figure S1, Supporting Information). Figure 1 shows the normalized UV−visible absorption and emission spectra of the composites using different initial dye concentrations, 1×10^{-2}, 1×10^{-3}, and 1×10^{-4} M (Figure S2, Supporting Information shows the nonnormalized UV−visible absorption spectra). The most diluted sample (1×10^{-4} M) exhibits a broad and structureless diffuse reflectance (DR) spectrum with an intensity maximum at 595 nm. The large width of the band at the half maximum of the intensity indicates the presence of several species of NR in the composites. The host material consists of a layered structure in which the dye can be located and interact with the units that form the framework. This suggests several possible orientations and positions of NR molecules in the MOF as well as interactions between them, resulting in several species. On the other hand, the emission spectrum of the 1×10^{-4} M sample excited at 470 nm shows a narrow band with a maximum at 645 nm. The narrow emission spectrum contrasts the broad DT one, which is explained in terms of the presence
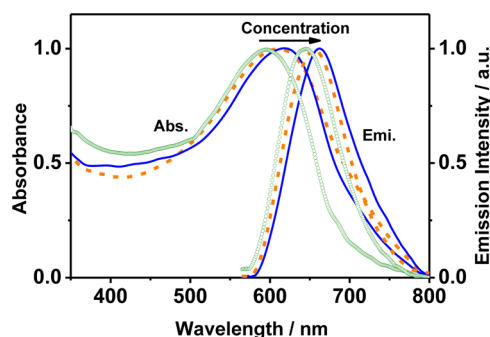

Figure 1. UV−visible absorption and emission spectra of NR interacting with Al−ITQ-HB at different initial dye concentrations: 1×10^{-4} M (green lines), 1×10^{-3} M (orange lines), and 1×10^{-2} M (blue lines). The emission spectra were recorded upon excitation at 550 nm.

of different NR populations in the MOF that are either nonemissive or weakly emissive and hence do not significantly contribute to the emission spectrum at this excitation wavelength (470 nm). To further understand the photobehavior of the composites, we recorded the steady-state spectra of two samples with larger initial dye concentrations: 1×10^{-3} and 1×10^{-2} M. The DR spectra show maxima at 611 and 618 nm, respectively (Figure 1). The shapes of the bands of the two concentrations are very similar but broader than that of the 1×10^{-4} M sample, which reflects the formation of aggregates at higher dye contents. The emission spectra of these two samples show a narrow band, exhibiting the intensity maximum at 655 and 665 nm, respectively. The red shift at increased concentrations supports the presence and emission of NR aggregates within the composites. The full width at half maximum (FWHM) of the emission bands are 2023, 2070, and 2125 cm^{-1} from the most diluted to the most concentrated sample, respectively. The trend in increasing the FWHM with the dye concentration also reflects the emission of additional species with significant contribution when the NR concentration increases. Studies of NR in SBMs have reported broader emission spectra and were explained in terms of enhanced contributions from the trapped emissive species in the materials.[29,31] Upon excitation at 470 nm, the emission of the three samples exhibits a green band (∼525 nm) (Figure S3, Supporting Information). We anticipate that this emission corresponds to the monomers, as we will show in the time-resolved emission spectra (TRES) (see below). The fluorescence excitation spectra gating the emission at 800 nm are well defined, with their intensity maxima at ∼610 nm (Figure S4, Supporting Information). Their shapes and maxima are similar to those of the DR spectra. However, the FWHM of the excitation spectra is smaller than that of the absorption ones, reflecting the presence of efficient nonradiative deactivation pathways at the excited state of some species of trapped NR molecules. Note that while gating the emission at 525 nm, we could not record an accurate excitation spectrum.

2.2. Picosecond Time-Resolved Fluorescence of NR@Al−ITQ-HB. *2.2.1. Nile Red Concentration Effect.* To understand the photodynamics of the NR@Al−ITQ-HB composites, we conducted time-resolved emission experiments with picosecond resolution. Figure 2 shows representative emission decays of samples at three different initial dye concentrations collected at different observation wavelengths (from 550 to 750 nm) and excited at 470 nm. Table 1 gives the
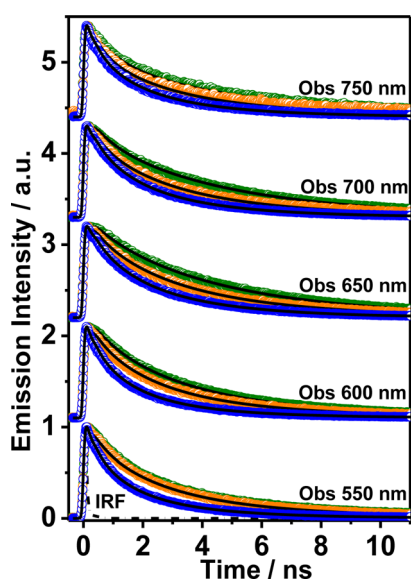
Figure 2. Normalized magic-angle emission decays of NR interacting with Al−ITQ-HB at different initial dye concentrations: 1×10^{-2} M (blue circles), 1×10^{-3} M (orange circles), and 1×10^{-4} M (green circles) upon excitation at 470 nm and different observation wavelengths. The solid lines are from the best global fit using a multiexponential function.

obtained time constants (τ_i), the pre-exponential factors (a_i), and relative contributions (c_i, normalized to 100) from multiexponential global fits. For the sample having 1×10^{-4} M NR initial concentration, we observed decay times of 0.71, 2.59, and 5.10 ns. The contribution of the shortest lifetime (0.71 ns) decreases as the observation wavelength increases, whereas the intermediate lifetime (∼2.6 ns) does not significantly vary throughout the emission spectrum. The contribution of the longest component (5.1 ns) increases with the observation wavelength. On the basis of these results and considering the steady-state observation, we assign the longest component to the emission lifetime of the monomers, which

undergo an ICT process to give a CS state. The emission lifetime of the photoproduced CS monomer is comparable to that reported for NR interacting with the SBMs (4.1 ns)[30] and in a dichloromethane (DCM) solution (4.4 ns).[28] We assign the intermediate component to NR aggregates interacting with the Al−ITQ-HB structure. Several studies have revealed that NR molecules easily form aggregates when encapsulated in restrictive environments.[30,38,39] For example, populations of both H- and J-type aggregates have been observed for NR in different porous materials such as zeolites and MCM-41.[37] The mean emission lifetime of the aggregates is ∼0.5 ns in NaY zeolites[31] and ∼1.2 ns in MCM-41,[30] which are significantly shorter than those observed in this composite (2.5 ns). The longer value observed in this system suggests the presence of different interactions between the dye species and the Al−ITQ-HB framework. Finally, we assign the shortest component (∼0.7 ns), which has its largest contribution at the blue part of the emission spectrum, to a monomer population that emits directly from the local-excited (LE) state, different from the ones having suffered an ICT (5.1 ns). Considering the structure of Al−ITQ-HB (Scheme 1), two different domains can be distinguished: (1) the linker domain, where the heptyl chains provide a quite nonpolar environment, and (2) another domain involving the aromatic and carboxylic groups and the metal clusters, where hydroxyl or oxy groups might be present, resulting in a higher polarity of the region. The occurrence of the ICT process in the interacting NR to produce CS species depends on the polar character of its local environment.[27,40,41] The LE state is stabilized in apolar media, increasing the energy barrier to the CS state and thus reducing the probability of the ICT event.[40−42] As a result, NR molecules in apolar media have a high probability to emit from the initial LE state. On the other hand, in polar environments, the energy barrier to reach the CS state decreases, making possible the occurrence of the ICT event and therefore, recording the emission signal from the photoproduced CS species. We suggest that the ∼5 ns component reflects the emission decay of those species. It has been reported that the ICT process occurs in hundreds of

Table 1. Values of the Fluorescence Emission Lifetimes (τ_i) and Normalized (to 100) Preexponential Factors (a_i) and Contributions ($c_i = \tau_i \times a_i$) Obtained from a Multiexponential Global Fit of the Emission Decays of NR@Al−ITQ-HB at Different Initial Dye Concentrations upon Excitation at 470 nm and Observation as Indicated

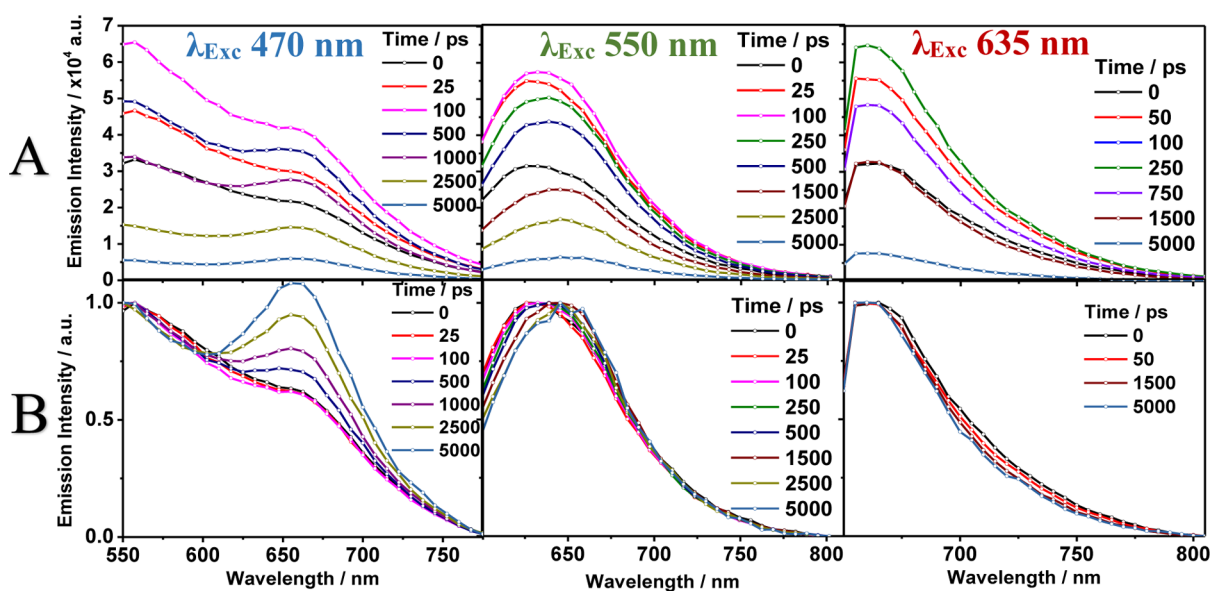| sample/M (initial dye concentration)	λ_{Obs}/nm	τ_1/ns (±0.05)	a_1	c_1	τ_2/ns (±0.20)	a_2	c_2	τ_3/ns (±0.20)	a_3	c_3
1×10^{-4}	525	**0.71**	34	19	**2.59**	38	35	**5.10**	28	46
	550		24	18		37	35		29	56
	600		14	3		41	31		45	66
	650		13	1		25	16		62	83
	700		14	4		17	11		69	85
	750		8	8		20	10		72	82
1×10^{-3}	525	**0.36**	25	4	**1.62**	35	26	**4.15**	40	70
	550		21	3		37	25		42	72
	600		16	2		43	28		41	70
	650		14	2		29	16		58	82
	700		15	4		30	19		46	77
	750		15	4		28	21		37	73
1×10^{-2}	525	**0.26**	30	7	**1.23**	45	37	**3.15**	25	56
	550		30	7		44	38		26	55
	600		27	6		45	40		28	54
	650		19	3		38	23		43	74
	700		21	3		40	28		39	69
	750		18	3		36	29		46	68

Figure 3. Nonnormalized (a) and normalized (b) TRES of NR@Al−ITQ-HB with 1×10^{-2} M initial dye concentration upon different excitation wavelengths and gating at the indicated delay times.

femtoseconds,[29−31] a time constant shorter than the time resolution of our time-correlated single-photon counting (TCSPC) technique (∼15 ps), and thus cannot be characterized. Another possible origin of the shortest component can be attributed to a NR population of weakly or nonemissive H-type aggregates. It has been reported that these types of aggregates of NR molecules in R-MCM41 have a lifetime of ∼0.3−0.4 ns.[29] The maximum contribution of this component is in the shortest wavelengths (suggesting an origin from the LE monomers). However, its contribution is still large at longer wavelengths (H-aggregate emission region). Thus, we suggest that the 0.7 ns component corresponds to a combined contribution of both LE and H-aggregate populations.

To further characterize the origin of the observed components, we prepared composites with different initial dye concentrations and studied their photobehaviors. Table 1 shows the values of the time constants obtained from multiexponential fits of the decays of the samples, in addition to the decay data discussed above. The lifetimes for the sample with 1×10^{-3} M dye are 0.36, 1.62, and 4.15 ns, whereas those of the sample with 1×10^{-2} M initial dye concentration are 0.26, 1.23, and 3.15 ns. The values of the emission lifetimes decrease with the NR concentration, and we explain it as a result of enhanced NR−NR interactions. The shortest lifetime is 0.26 ns in the most concentrated sample (0.7 ns for the least concentrated one). Two observations can be made: first, the lifetimes at higher initial NR concentrations are comparable to those reported for H-aggregates in R-MCM-41 (0.3−0.4 ns).[29] Second, the large difference between the value of this time component (∼0.7 ns) in the most diluted sample and the one (0.26 ns) at higher concentrations suggests that at lower concentrations, the component arises mostly from LE monomers, whereas at higher ones, it comes from the H-type aggregates. A similar trend is observed for the other two lifetimes: the intermediate value, which we previously assigned to J-aggregates, decreases from 2.59 to 1.23 ns, whereas the lifetime assigned to the CS state changes from 5.10 to 3.15 ns. The shortening in the lifetime values is explained in terms of the interactions of neighboring NR species that provoke a self-

emission quenching as it has been shown when NR interacts within other materials.[29,30] The contribution of the longest lifetime assigned to the CS monomer species decreases at larger NR contents, as a result of aggregate formation.

2.2.2. Time-Resolved Emission Spectra. To further elucidate the composite photodynamics and to interrogate the different NR species present in this MOF, we recorded the TRES of the most concentrated sample at different excitation wavelengths. Figure 3 shows the TRES of samples that are nonnormalized and normalized to the maximum of emission intensities. Exciting at 470 nm results in a band with a maximum at ∼550 nm and a second one at ∼650 nm. The greenest band decays, reaching its half-maximum of intensity between 500 and 700 ps, which, following the results obtained from the analysis of the emission decays, corresponds to the combined emission of LE monomers and H-aggregates. The second band is a combination of the emissions of the CS monomer and the J-aggregate populations. When the sample is excited at 550 nm, the greenest band is not observed. The normalized TRES indicates that at shorter gating times (100 ps to 1 ns), the band is broader, but it becomes narrower at longer observation times. This suggests that at short gating times, the emission comes from several species. Furthermore, the maximum of this band shifts from ∼625 to 670 nm, which suggests that two overlapping bands contribute to the emission spectrum. The spectral and TCSPC results indicate that these two bands correspond to the CS monomer and J-aggregates. The TRES of the composites were also collected upon excitation at 635 nm. These spectra correspond to the aggregates as the monomers do not absorb at this wavelength of excitation. The TRES show a band with a maximum at ∼665 nm and not changing with time, suggesting that it mainly corresponds to the emission of J-aggregates. To study the presence of possible processes and the relations between the excited species of the system, we also constructed time-resolved area-normalized emission spectra (TRANES).[43] Figure 4 shows the TRANES of the most concentrated sample upon a 470 nm excitation. The isoemissive point at 625 nm confirms an excited-state process bridging the species that emit at 550 and 650 nm. As explained earlier, NR
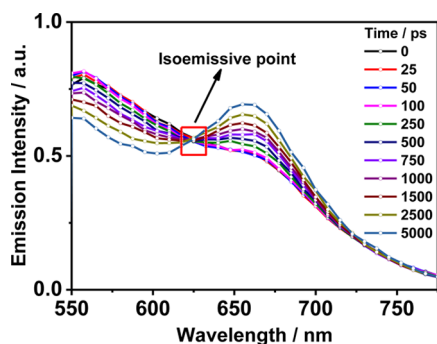
Figure 4. TRANES of NR@Al−ITQ-HB with 1×10^{-2} M initial dye concentration upon 470 nm of excitation wavelength and gating at the indicated delay times.

monomers can undergo ICT from the LE state (550 nm band) to give the CS state which emits at wavelengths longer than 650 nm. Time-resolved studies have reported that this process occurs in tens to hundreds of femtoseconds.[29,31]

2.3. Femtosecond Time-Resolved Fluorescence of NR@Al−ITQ-HB.

To further elucidate the photodynamics of NR@Al−ITQ-HB, we recorded the fluorescence signal of the most concentrated sample in the solid state using femtosecond resolution. Figure 5 shows the emission transients of the sample
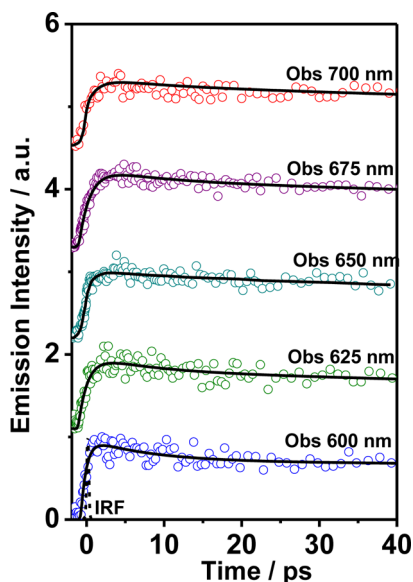

Figure 5. Femtosecond emission transients of NR@Al−ITQ-HB with 1×10^{-2} M initial dye concentration in the solid state upon excitation at 470 nm and observation at different wavelengths. The fs-emission transients were recorded using the reflection mode (see Supporting Information). The solid line is from the best-fit using a multi-exponential function.

at representative observation wavelengths upon excitation at 470 nm. Table 2 shows the time constants (τ_i) and their contributions (a_i, normalized to 100) to the signal after a multiexponential fit. The transients are composed of three components, each with different time constant: ~1, ~8.2, and 260 ps. The 260 ps component was fixed in the fit using the values obtained from the ps emission decays. The intermediate one, with a time of ~8.2 ps, is present at all the observation wavelengths. This component is assigned to VC of NR. The time constant of the VC of NR in SBMs was reported to be

Table 2. Values of the Time Constants and Normalized (to 100) Preexponential Factors (a_i) Obtained from a Multiexponential Fit of the Femtosecond Emission Transients of NR@Al−ITQ-HB with 1×10^{-2} M Initial Dye Concentration upon Excitation at 470 nm and Observation as Indicated

λ_{Obs}/nm	τ_1/ps (±0.05)	a_1[a]	τ_2/ps (±0.20)	a_2	τ_3/ps	a_3
600	0.8	10	8.1	20		70
625	0.9	−100	8.0	22		78
650	1.1	−100	8.5	5	260[b]	95
675	1.0	−100	8.2	4		96
700	1.3	−100				100

[a]The negative sing for a_i indicates a rising component in the emission signal. [b]Fixed value in the fit.

~2−3 ps.[29−31] The large difference in the values of this component can be explained by the presence of hydroxyl groups in SBMs that interact with NR via H-bonds, favoring vibrational energy transfer from excited NR molecules to the surrounding environment. In the present composites, the NR@Al−ITQ-HB complexes are formed through weaker, non-specific interactions that, combined with the confinement effect caused by the laminar MOF structure, result in slower excess energy dissipation. Finally, the shortest component (~1 ps) is present at 600 nm (higher energy of the emission spectrum), and its signal is rising at 625 nm. Figure S5 (Supporting Information) shows the presence of this rise in the component when observing at 675 nm. This decay at short wavelengths and rise at longer ones suggest a common origin of the process associated with this component. NR in solution and encapsulated within SBM undergoes ultrafast ICT from its amino group to its oxo one. This event occurs in ~1 ps in DCM solution, and it is favored in polar media.[26] Upon encapsulation in SBM, the NR ICT reaction becomes faster, exhibiting a time constant of hundreds of fs.[30,31,39] The relatively long time observed here (~1 ps), associated with ICT in NR@Al−ITQ-HB, might reflect that NR molecules undergoing ICT are located in a more apolar environment. The similar values of the ICT time constant in both DCM and this MOF suggest that the polarities of the two media are not very different.

2.4. Scanning Confocal Fluorescence Microscopy of NR@Al−ITQ-HB.

To further characterize the photobehavior of the composites, we used fluorescence lifetime imaging microscopy (FLIM). NR@Al−ITQ-HB crystals of different sizes were selected under the microscope and studied. The fluorescence decays were measured upon a 470 nm excitation and collected in two spectral regions: 590−640 and 645−800 nm. To begin with, Figure 6A shows the emission decays of single crystals (less than 0.5 μm in diameter), and the inset exhibits the corresponding FLIM image. Table 3 gives the time constants (τ_i) and the pre-exponential factors (a_i, normalized to 100) obtained from multiexponential global fits of the emission decays of single-crystals, as well as the values obtained for agglomerates (multiple crystals joined) under the same experimental conditions. The biexponential fits give lifetimes of 1.53 and 3.60 ns for single crystal observations. The two components are assigned to the emissions of J-aggregates and monomers, respectively, as the lifetime values are comparable to the ones (1.23 and 3.15 ns, respectively) obtained in the previous TCSPC experiments using the ensemble solid composites. The component contribution depends on the
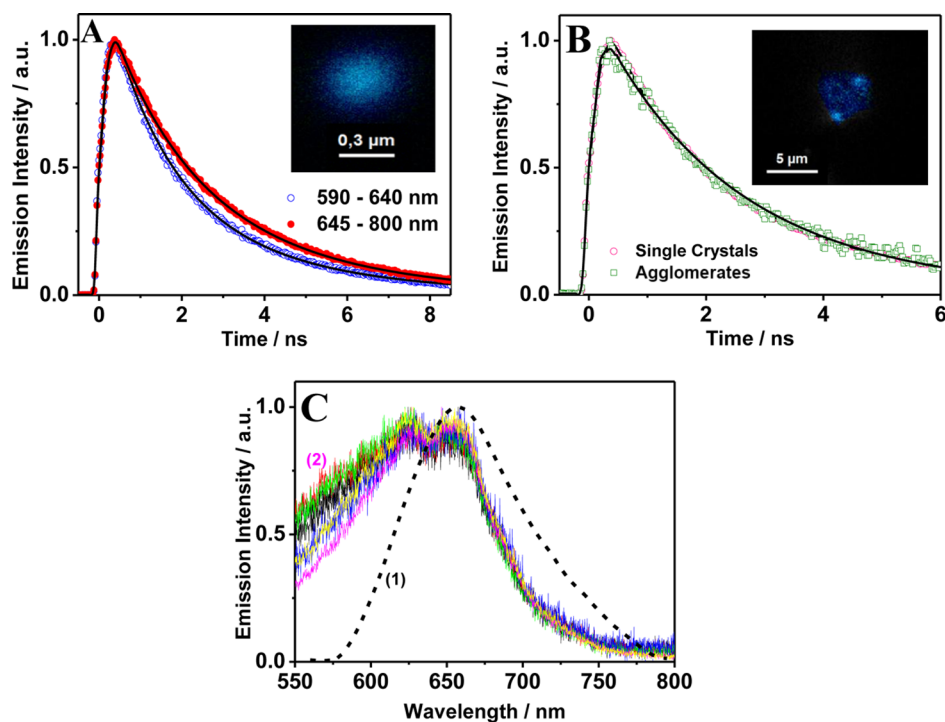
Figure 6. (a) Decays of the NR@Al−ITQ-HB single crystals with 1×10^{-2} M initial dye concentration. The inset shows an image of a single crystal. The excitation wavelength was 470 nm, and the decays were recorded at different observation wavelength regions, as indicated in the figure. The solid lines are from the best fit using a multiexponential function. (b) Comparison of the decays of single crystals and agglomerates measured under the same experimental conditions. The solid line is from the best fit using a multiexponential function. The inset shows an image of an agglomerate. (c) Emission spectra of NR@Al−ITQ-HB with 1×10^{-2} M initial dye concentration of the (1) ensemble solid and (2) many single crystals and agglomerates upon excitation at 470 nm.

Table 3. Comparison of the Single Crystal and Agglomerate Fluorescence Emission Lifetimes (τ_i) and Normalized (to 100) Preexponential Factors (a_i) Obtained from a Multiexponential Fit of the Emission Decays of NR@Al−ITQ-HB with 1×10^{-2} M initial dye concentration of the sample upon excitation at 470 nm

Sample	λ_{Obs}/nm	τ_1/ns (± 0.05)	a_1	τ_2/ns (± 0.20)	a_2
single crystals	590−640	1.53	65	3.60	35
	645−800		52		48
agglomerates	590−800	1.47	56	3.51	44

observed spectral region, with the shortest being the one that contributes the most to the blue side of the spectrum. Figure 6B shows a comparison between the fluorescence emission decays from single crystals and those from the agglomerates under the microscope. We observe the same decay behavior for both systems; therefore, we can consider that NR is not affected by intercrystal interactions. It should be noted that the shortest component observed in the ensemble solid is not seen in these decays. This can be explained by the longer time resolution (~300 ps) of the microscope setup, compared to the TCSPC system (~70 ps). Figure 6C shows a comparison between the emission spectra of many single crystals and agglomerates and the ensemble solid one. Whereas the latter displays a unique band with a maximum at 665 nm, single crystal and agglomerate spectra show two maxima of equal intensity, at 637 nm and 663 nm. The emission spectra of single and many crystals indicate that different emitting species of NR are present within this MOF. The region of ~575 nm shows a clear variation in the intensity which does not depend on the size or

agglomeration of the measured crystal. However, we can observe a difference in the intensities in this region when comparing with the ensemble solid spectrum. This fact can be explained by the absorption of the crystal emission by a neighboring crystal in the ensemble solid because of the significant spectral overlap between the absorption and emission bands.

3. CONCLUSIONS

In this work, we have presented studies of the photoproperties of a novel composite formed by an MOF-type material, Al−ITQ-HB, and NR using steady-state and time-resolved spectroscopies. The composites contain several NR populations whose contributions in the emission signal are affected by the initial dye concentration used to make the complexes. The different species are assigned to J- and H-type aggregates and monomers. The parts that form the Al−ITQ-HB framework, linkers and metal clusters, provide environments that are sufficiently different to affect the NR dynamics. We identify two types of NR monomers: one that emits from the LE state (~0.7 ns) and another one showing an ICT process to give a CS state that has a lifetime of ~5 ns. Femtosecond experiments unravel the formation of the CS state in ~1 ps. The VC of the trapped species occurs in ~8.2 ps. These processes are significantly longer than those observed for NR when it interacts with SBMs. The less polar character of the MOF and the weak interactions that the layered structure provides affect the observed behavior. Finally, FLIM studies on single crystals and agglomerates reveal a homogenous distribution of lifetimes within the composites. The increment in the intensity of the green part of the emission spectra measured under the

microscope comparing with the ensemble solid one reveals self-absorption of the emission from the latter.

These findings demonstrate that the different environments in the Al−ITQ-HB structure affect the behavior of this classical molecular probe interacting with the framework. The results will aid in the design of materials for different nanomaterial applications.

4. EXPERIMENTAL SECTION

4.1. Synthesis of the NR@M-ITQ MOFs. The material was prepared according to the procedures reported in the bibliography.[22] Briefly, Al−ITQ-HB was synthesized from equimolar quantities of $AlCl_3 \cdot 6H_2O$ (3.1 mmol) and 4-heptylbenzoic acid (3.1 mmol), which had each been dissolved in 15 mL of dimethylformamide. The two solutions were mixed, and the resulting slurry was introduced into a stainless-steel autoclave and heated at 150 °C for 24 h under autogenous pressure and static conditions. Once cooled to room temperature, the solution was filtered with distilled water. The sample was activated in methanol for 24 h to efficiently remove the unreacted linker and solvent molecules. The material was then isolated and dried under vacuum at room temperature. Its structure was observed through transmission electron microscopy (TEM) micrographs (Figure S6, Supporting Information), which were obtained with a JEOL JEM2100F electron microscope operating at 200 keV. The samples were prepared directly by dispersing the powders onto carbon copper grids. The dye NR (Sigma-Aldrich, purity >98.0%) was incorporated into the material for spectroscopic studies. First, dichloromethane solutions of the dye with specific molar concentrations (1×10^{-2}, 1×10^{-3}, and 1×10^{-4} M) were prepared. Then, 50 mg of the MOF was added to 1 mL of the dye solution, and the mixture was stirred for 24 h at room temperature. The material was washed several times until no trace of NR was observed in the UV−visible absorption spectra of the supernatant. Finally, the material was dried to eliminate the solvent. The loadings obtained from the supernatant absorption measurements were 1.8×10^{18}, 2.3×10^{17}, and 3.2×10^{16} NR molecules/g_{MOF} for 1×10^{-2}, 1×10^{-3}, and 1×10^{-4} M initial dye concentrations, respectively.

4.2. Structural, Spectroscopic, and Dynamics Measurements. Steady-state UV−visible absorption and fluorescence measurements were conducted using JASCO V-670 and FluoroMax-4 (Jobin-Yvon) spectrophotometers, respectively. The diffuse reflectance spectra were measured using a 60 mm integrating sphere (ISN-723) and corrected with the Kubelka−Munk function. Picosecond time-resolved emission experiments were recorded employing a TSCPC system.[44] The samples were excited by 40 ps pulsed (~1 mW, 40 MHz repetition rate) diode lasers (PicoQuant) centered at 470, 550, and 635 nm. The instrument response function (IRF) of the diode laser was approximately 70 ps wide. The fluorescence signal was collected at the magic angle (54.71°) and monitored from 90° from the excitation beam at discrete emission wavelengths. The decays were deconvoluted and fitted to a multiexponential function using the FLUOFIT package (PicoQuant), which allowed single and global fits. The quality of the fits as well as the number of exponentials were carefully selected based on the reduced χ^2 values (which were always below <1.2) and the distributions of the residuals. All of the experiments were performed at room temperature (295 K). Femtosecond time-resolved emission decays were collected using a fluorescence upconversion technique in the solid state

with a reflection mode disposition of the system. The setup of the equipment and a detailed description of the system is explained in the Supporting Information (Figure S7). Briefly, the sample was excited at 470 nm and recorded at different observation wavelengths. To analyze the fs-transients, we deconvoluted a multiexponential function with the IRF to fit the experimental data. The errors for the calculated time components were smaller than 15% in all cases. The confocal microscopy measurements were performed on a MicroTime 200 confocal microscope (PicoQuant). The excitation was conducted with the same diode laser used in the TSCPC experiment. The emission signal was collected using a 520 nm long pass filter (Chroma). In brief, the instrument consists of an inverse Olympus IX 71 microscope equipped with a water-immersion objective (×60 NA1.2, Olympus) and a 2D piezo scanner (Physik Instrumente). The emitted light was then focused on a 50 μm pinhole and later collimated to two independent single-photon avalanche photodiodes (Micro-Photon-Devices) for the time-resolved measurements. The emission spectra were collected through a Shamrock ST-303i (Andor Technology) imaging spectrograph and detected by an Andor Newton EMCCD camera (Andor Technology). The samples were measured in the solid state, which was prepared by spilling a small amount of the solid powder over the coverslip and introducing it into the sample holder. Fifteen single crystals and agglomerates were analyzed.

■ ASSOCIATED CONTENT

Ⓢ Supporting Information

The Supporting Information is available free of charge on the ACS Publications website at DOI: 10.1021/acsomega.7b01718.

> UV−visible absorption spectra of Al−ITQ-HB in the solid state; absorption spectra of NR@Al−ITQ-HB with different initial dye concentrations; emission and excitation spectra, respectively, of the NR@Al−ITQ-HB composites; normalized emission transient decay of the most concentrated NR@Al−ITQ-HB composite upon excitation at 470 nm and observation at 675 nm; TEM images of Al−ITQ-HB; scheme of the optics for upconversion experiments in the reflection mode (PDF)

■ AUTHOR INFORMATION

Corresponding Authors

*E-mail: udiaz@itq.upv.es. Phone: +34-963-877811 (U.D.).
*E-mail: Abderrazzak.Douhal@uclm.es. Phone: +34-925-265717 (A.D.).

ORCID ◉

Boiko Cohen: 0000-0002-5400-4678
Avelino Corma: 0000-0002-2232-3527
Urbano Díaz: 0000-0003-1472-8724
Abderrazzak Douhal: 0000-0003-2247-7566

Notes

The authors declare no competing financial interest.

■ REFERENCES

(1) Kaskel, S. Porous Metal-Organic Frameworks. *Handbook of Porous Solids*; Wiley-VCH Verlag GmbH, 2008; pp 1190−1249.

(2) Kitagawa, S.; Kitaura, R.; Noro, S.-i. Functional Porous Coordination Polymers. *Angew. Chem., Int. Ed.* **2004**, *43*, 2334−2375.

(3) Rowsell, J. L. C.; Yaghi, O. M. Metal−organic frameworks: a new class of porous materials. *Microporous Mesoporous Mater.* **2004**, *73*, 3−14.

(4) Corma, A. From Microporous to Mesoporous Molecular Sieve Materials and Their Use in Catalysis. *Chem. Rev.* **1997**, *97*, 2373−2420.

(5) Czaja, A. U.; Trukhan, N.; Müller, U. Industrial applications of metal-organic frameworks. *Chem. Soc. Rev.* **2009**, *38*, 1284−1293.

(6) Getman, R. B.; Bae, Y.-S.; Wilmer, C. E.; Snurr, R. Q. Review and analysis of molecular simulations of methane, hydrogen, and acetylene storage in metal-organic frameworks. *Chem. Rev.* **2012**, *112*, 703−723.

(7) Li, B.; Wen, H.-M.; Wang, H.; Wu, H.; Tyagi, M.; Yildirim, T.; Zhou, W.; Chen, B. A porous metal-organic framework with dynamic pyrimidine groups exhibiting record high methane storage working capacity. *J. Am. Chem. Soc.* **2014**, *136*, 6207−6210.

(8) Li, J.-R.; Kuppler, R. J.; Zhou, H.-C. Selective gas adsorption and separation in metal-organic frameworks. *Chem. Soc. Rev.* **2009**, *38*, 1477−1504.

(9) Murray, L. J.; Dincă, M.; Long, J. R. Hydrogen storage in metal-organic frameworks. *Chem. Soc. Rev.* **2009**, *38*, 1294−1314.

(10) Li, J.-R.; Sculley, J.; Zhou, H.-C. Metal−Organic Frameworks for Separations. *Chem. Rev.* **2012**, *112*, 869−932.

(11) Ma, L.; Abney, C.; Lin, W. Enantioselective catalysis with homochiral metal-organic frameworks. *Chem. Soc. Rev.* **2009**, *38*, 1248−1256.

(12) Liu, J.; Chen, L.; Cui, H.; Zhang, J.; Zhang, L.; Su, C.-Y. Applications of metal-organic frameworks in heterogeneous supra-molecular catalysis. *Chem. Soc. Rev.* **2014**, *43*, 6011−6061.

(13) Horcajada, P.; Gref, R.; Baati, T.; Allan, P. K.; Maurin, G.; Couvreur, P.; Férey, G.; Morris, R. E.; Serre, C. Metal−Organic Frameworks in Biomedicine. *Chem. Rev.* **2012**, *112*, 1232−1268.

(14) Kurmoo, M. Magnetic metal-organic frameworks. *Chem. Soc. Rev.* **2009**, *38*, 1353−1379.

(15) Foster, M. E.; Azoulay, J. D.; Wong, B. M.; Allendorf, M. D. Novel metal-organic framework linkers for light harvesting applications. *Chem. Sci.* **2014**, *5*, 2081−2090.

(16) Klein, N.; Herzog, C.; Sabo, M.; Senkovska, I.; Getzschmann, J.; Paasch, S.; Lohe, M. R.; Brunner, E.; Kaskel, S. Monitoring adsorption-induced switching by 129Xe NMR spectroscopy in a new metal-organic framework Ni2(2,6-ndc)2(dabco). *Phys. Chem. Chem. Phys.* **2010**, *12*, 11778−11784.

(17) Chughtai, A. H.; Ahmad, N.; Younus, H. A.; Laypkov, A.; Verpoort, F. Metal-organic frameworks: versatile heterogeneous catalysts for efficient catalytic organic transformations. *Chem. Soc. Rev.* **2015**, *44*, 6804−6849.

(18) Loiseau, T.; Serre, C.; Huguenard, C.; Fink, G.; Taulelle, F.; Henry, M.; Bataille, T.; Férey, G. A Rationale for the Large Breathing of the Porous Aluminum Terephthalate (MIL-53) Upon Hydration. *Chem.—Eur. J.* **2004**, *10*, 1373−1382.

(19) Klein, N.; Hoffmann, H. C.; Cadiau, A.; Getzschmann, J.; Lohe, M. R.; Paasch, S.; Heydenreich, T.; Adil, K.; Senkovska, I.; Brunner, E.; Kaskel, S. Structural flexibility and intrinsic dynamics in the M2(2,6-ndc)2(dabco) (M = Ni, Cu, Co, Zn) metal-organic frameworks. *J. Mater. Chem.* **2012**, *22*, 10303−10312.

(20) Hoffmann, H. C.; Assfour, B.; Epperlein, F.; Klein, N.; Paasch, S.; Senkovska, I.; Kaskel, S.; Seifert, G.; Brunner, E. High-Pressure in Situ 129Xe NMR Spectroscopy and Computer Simulations of Breathing Transitions in the Metal−Organic Framework Ni2(2,6-ndc)2(dabco) (DUT-8(Ni)). *J. Am. Chem. Soc.* **2011**, *133*, 8681−8690.

(21) Yang, Q.; Vaesen, S.; Vishnuvarthan, M.; Ragon, F.; Serre, C.; Vimont, A.; Daturi, M.; De Weireld, G.; Maurin, G. Probing the adsorption performance of the hybrid porous MIL-68(Al): a synergic combination of experimental and modelling tools. *J. Mater. Chem.* **2012**, *22*, 10210−10220.

(22) García-García, P.; Moreno, J. M.; Díaz, U.; Bruix, M.; Corma, A. Organic−inorganic supramolecular solid catalyst boosts organic reactions in water. *Nat. Commun.* **2016**, *7*, 10835.

(23) Choi, M.; Na, K.; Kim, J.; Sakamoto, Y.; Terasaki, O.; Ryoo, R. Stable single-unit-cell nanosheets of zeolite MFI as active and long-lived catalysts. *Nature* **2009**, *461*, 246−249.

(24) Moreno, J. M.; Navarro, I.; Díaz, U.; Primo, J.; Corma, A. Single-Layered Hybrid Materials Based on 1D Associated Metalorganic Nanoribbons for Controlled Release of Pheromones. *Angew. Chem., Int. Ed.* **2016**, *55*, 11026−11030.

(25) Cser, A.; Nagy, K.; Biczók, L. Fluorescence lifetime of Nile Red as a probe for the hydrogen bonding strength with its microenvironment. *Chem. Phys. Lett.* **2002**, *360*, 473−478.

(26) Dutta, A. K.; Kamada, K.; Ohta, K. Spectroscopic studies of nile red in organic solvents and polymers. *J. Photochem. Photobiol., A* **1996**, *93*, 57−64.

(27) Freidzon, A. Y.; Safonov, A. A.; Bagaturyants, A. A.; Alfimov, M. V. Solvatofluorochromism and twisted intramolecular charge-transfer state of the nile red dye. *Int. J. Quantum Chem.* **2012**, *112*, 3059−3067.

(28) Sarkar, N.; Das, K.; Nath, D. N.; Bhattacharyya, K. Twisted charge transfer processes of nile red in homogeneous solutions and in faujasite zeolite. *Langmuir* **1994**, *10*, 326−329.

(29) Martín, C.; Piatkowski, P.; Cohen, B.; Gil, M.; Navarro, M. T.; Corma, A.; Douhal, A. Ultrafast Dynamics of Nile Red Interacting with Metal Doped Mesoporous Materials. *J. Phys. Chem. C* **2015**, *119*, 13283−13296.

(30) Martin, C.; Cohen, B.; Navarro, M. T.; Corma, A.; Douhal, A. Unraveling the ultrafast behavior of nile red interacting with aluminum and titanium co-doped MCM41 materials. *Phys. Chem. Chem. Phys.* **2016**, *18*, 2152−2163.

(31) di Nunzio, M. R.; Caballero-Mancebo, E.; Martín, C.; Cohen, B.; Navarro, M. T.; Corma, A.; Douhal, A. Femto-to nanosecond photodynamics of Nile Red in metal-ion exchanged faujasites. *Microporous Mesoporous Mater.* **2018**, *256*, 214−226.

(32) Datta, A.; Mandal, D.; Pal, S. K.; Bhattacharyya, K. Intramolecular Charge Transfer Processes in Confined Systems. Nile Red in Reverse Micelles. *J. Phys. Chem. B* **1997**, *101*, 10221−10225.

(33) Hazra, P.; Chakrabarty, D.; Chakraborty, A.; Sarkar, N. Intramolecular charge transfer and solvation dynamics of Nile Red in the nanocavity of cyclodextrins. *Chem. Phys. Lett.* **2004**, *388*, 150−157.

(34) Maiti, N. C.; Krishna, M. M. G.; Britto, P. J.; Periasamy, N. Fluorescence Dynamics of Dye Probes in Micelles. *J. Phys. Chem. B* **1997**, *101*, 11051−11060.

(35) Martin, C.; Bhattacharyya, S.; Patra, A.; Douhal, A. Single and multistep energy transfer processes within doped polymer nano-particles. *Photochem. Photobiol. Sci.* **2014**, *13*, 1241−1252.

(36) Martin, C.; di Nunzio, M. R.; Cohen, B.; Douhal, A. Location and freedom of single and double guest in dye-doped polymer nanoparticles. *Photochem. Photobiol. Sci.* **2014**, *13*, 1580−1589.

(37) Alarcos, N.; Cohen, B.; Ziółek, M.; Douhal, A. Photochemistry and Photophysics in Silica-Based Materials: Ultrafast and Single Molecule Spectroscopy Observation. *Chem. Rev.* **2017**, *117*, 13639−13720.

(38) Felbeck, T.; Behnke, T.; Hoffmann, K.; Grabolle, M.; Lezhnina, M. M.; Kynast, U. H.; Resch-Genger, U. Nile-Red−Nanoclay Hybrids: Red Emissive Optical Probes for Use in Aqueous Dispersion. *Langmuir* **2013**, *29*, 11489−11497.

(39) Martín, C.; Piatkowski, P.; Cohen, B.; Gil, M.; Navarro, M. T.; Corma, A.; Douhal, A. Ultrafast Dynamics of Nile Red Interacting with Metal Doped Mesoporous Materials. *J. Phys. Chem. C* **2015**, *119*, 13283−13296.

(40) Jee, A.-Y.; Park, S.; Kwon, H.; Lee, M. Excited state dynamics of Nile Red in polymers. *Chem. Phys. Lett.* **2009**, *477*, 112−115.

(41) Guido, C. A.; Mennucci, B.; Jacquemin, D.; Adamo, C. Planar vs. twisted intramolecular charge transfer mechanism in Nile Red: new hints from theory. *Phys. Chem. Chem. Phys.* **2010**, *12*, 8016−8023.

(42) Freidzon, A. Y.; Safonov, A. A.; Bagaturyants, A. A.; Alfimov, M. V. Solvatofluorochromism and twisted intramolecular charge-transfer state of the nile red dye. *Int. J. Quantum Chem.* **2012**, *112*, 3059−3067.

(43) Koti, A. S. R.; Krishna, M. M. G.; Periasamy, N. Time-Resolved Area-Normalized Emission Spectroscopy (TRANES): A Novel Method for Confirming Emission from Two Excited States. *J. Phys. Chem. A* **2001**, *105*, 1767−1771.

(44) Organero, J. A.; Tormo, L.; Douhal, A. Caging ultrafast proton transfer and twisting motion of 1-hydroxy-2-acetonaphthone. *Chem. Phys. Lett.* **2002**, *363*, 409−414.